The Effects of Flash-Weakening and Damage on the Evolution of Fault Strength and Temperature

A. W. Rempel

Department of Geological Sciences, University of Oregon, Eugene, Oregon, USA

The effects of fluid pressurization in altering the fault strength and limiting the temperature rise during earthquake slip are modeled for the case of a thin, but finite, shear zone, with state-dependent properties that are chosen to represent conditions along a mature fault at moderate seismogenic depth. We include the effects of flash-weakening at highly stressed asperity contacts by extending the model of Rice [1999; 2006] to treat the relative motion between gouge particles as equal to either 1) the slip rate or 2) the product of the particle diameter and the strain rate. At slips exceeding a few centimeters, the strength evolution is relatively insensitive to the difference between these two formulations, but the predicted temperature rise is considerably greater for the strain-rate dependent case. Our calculations demonstrate how increasing levels of damage can significantly limit the reduction in fault strength, resulting in more rapid heating and ultimately leading to the predicted onset of melting following relatively modest slips.

1. INTRODUCTION

The mechanical work performed during an increment of slip along a fault segment is given by the product of the segment area and slip distance with the resisting fault strength. Over the duration of an earthquake, the sum of this work can be equated with the difference between the change in stored energy and the total heat released in all its forms [e.g. see Kanamori and Rivera, 2006; Cocco et al., 2006]. Hence, the manner in which the fault strength evolves is one of the key factors that controls the energy budget of an earthquake. The potential for pore fluids to control the strength of mature fault zones during earthquake slip is well established [e.g. Sibson, 1973; Lachenbruch, 1980; Mase and Smith, 1985, 1987]. Recent advances on several fronts have prompted renewed efforts to constrain these effects, commonly referred to as *thermal pressurization*, with a new generation of fault-zone models [e.g. Andrews, 2002; Rice and Cocco, 2005; Rice, 2006; Rempel and Rice, 2006; Bizzarri and Cocco, 2006a,b].

These models benefit, in particular, from detailed studies of shear localization along mature fault zones, which exhibit layers of concentrated slip, or principal slip surfaces (PSS), that are much thinner than had previously been widely appreciated—typically of millimeter scale or less [Chester and Chester, 1998; Chester and Goldsby, 2003; Chester et al., 2003, 2004; Sibson, 2003; Wibberley and Shimamoto, 2003, 2005; Noda and Shimamoto, 2005; Shipton et al., 2006a,b]. Measurements of transport properties [Lockner et al., 2000; Wibberley, 2002; Wibberley and Shimamoto, 2003] suggest that this is much less than the characteristic distance over which the pore pressure changes, and comparable to the characteristic distance over which the temperature changes.

Innovative experiments at several laboratories have begun to access the combinations of high slip-rates and confining stresses that characterize those that operate during earthquakes [Tsatsumi and Shimamoto, 1997; Goldsby and Tullis, 2002; Tullis and Goldsby, 2003a,b; Di Toro et al., 2004, 2006; Roig Silva et al., 2004; Prakash, 2004; Prakash and Yuan, 2004; Hirose and Shimamoto, 2005]. In addition to

Earthquakes: Radiated Energy and the Physics of Faulting
Geophysical Monograph Series 170

10.1029/170GM26

identifying new weakening mechanisms, such as the creation of silica gels, and even potential strengthening effects associated with the onset of melt, a dramatic reduction in the effective friction coefficient is observed that is both distinct from these effects and likely fundamental to the frictional behavior of solids in general as they near their melting temperatures. In analogy with the high-speed frictional behavior of metals [e.g. Bowden and Thomas, 1954], the "flash-weakening" mechanism proposed by Rice [1999] has been developed and applied to explain these observations and also to further constrain frictional behavior in modeling efforts [Beeler and Tullis, 2003; 2006; Rice and Cocco, 2006; Rice, 2006; Rempel and Rice, 2006]. As detailed further below, flash-weakening is the term given to the reduction in effective strength that is caused by transient heating and weakening at micron-scale asperity contacts.

The extreme localization identified in exhumed fault zones prompted Rice [2006] to propose an approximate analytical model for the constitutive behavior of fluid-saturated gouge that is sheared along a planar boundary. Comparisons with a generalized numerical treatment for shear in a finite layer support the planar-slip approximation for predicting the fault strength and fracture energy [Rempel and Rice, 2006]. However, the increase in fault zone temperature that is produced by shear heating is quite sensitive to the width of the shearing layer h. The case of slip on a plane provides an upper bound on the temperature rise, but the need for improved understanding of the dynamic interactions that control h is highlighted by these modeling studies [see also Rice and Rudnicki, 2006; Shipton et al., 2006b].

Rapid changes to the pore pressure and temperature as a consequence of thermal pressurization produce corresponding changes in fault zone properties that affect the fluid and heat transport. The dominant effect is to reduce near-axis gradients in pore pressure, leading to increased strength and more rapid temperature rise than would be predicted for a shear zone characterized by its properties in the ambient state [Rempel and Rice, 2006]. Here, we examine these effects further and focus in particular on the role of fault-zone damage and temperature-dependent flash-weakening in determining how fault strength and temperature evolve due to thermal pressurization. A kinematic model is used to simplify the analysis and enable us to isolate the effects of these particular phenomena; in consequence we omit several important, but otherwise distracting effects, such as the changes in slip rate that accompany dynamic rupture [e.g. Bizarri and Cocco, 2006a,b]. A brief description of the modeling procedure is given in the next section, together with a discussion of the relevant parameters. We then present a sequence of model predictions before summarizing our results and discussing their implications.

2. MODEL DESCRIPTION

We solve the conservation equations to predict the evolution of temperature and pore pressure in response to an imposed rate of shear. We assume that during the slip event, transport of heat and pore fluid is only in the direction normal to the symmetry plane, which we define as the origin; the Lagrangian coordinate y is used to measure distance into the surrounding gouge (see figure 1). Taking account of conductive heat transport (thermal diffusivity α_{th}, volumetric heat capacity ρc), Darcian fluid transport (hydraulic diffusivity α_{hy}, storage capacity β), and the thermo-poroelastic behavior of the gouge (expansion ratio Λ), shear heating causes the temperature $T(y,t)$ and pore pressure $P(y,t)$ to evolve according to [e.g. Rice, 2006; Rempel and Rice, 2006]

$$\frac{\partial T}{\partial t} = \alpha_{th}\frac{\partial^2 T}{\partial y^2} + \frac{1}{\rho c}\frac{\partial T}{\partial y}\frac{\partial}{\partial y}\left(\rho c\ \alpha_{th}\right) + \frac{\tau\dot{\gamma}}{\rho c} \qquad (1)$$

$$\frac{\partial P}{\partial t} = \alpha_{hy}\frac{\partial^2 P}{\partial y^2} + \frac{1}{\beta}\frac{\partial P}{\partial y}\frac{\partial}{\partial y}\left(\beta\alpha_{hy}\right) + \Lambda\frac{\partial T}{\partial t}\,. \qquad (2)$$

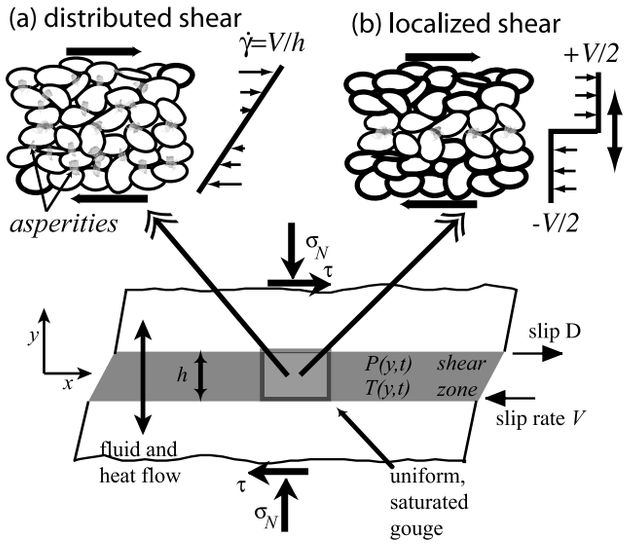

Figure 1. A schematic diagram of the shear zone. As discussed further in the text, two models of flash-weakening are considered. In (a) shear is evenly distributed through a zone of thickness h at uniform strain rate $\dot{\gamma}$. By contrast in (b), shear is completely localized and concentrated at fewer asperity contacts at any given time, though the plane of localization moves about during the earthquake in a zone of the same overall thickness h. This thickness, while small, is assumed to greatly exceed the sizes of individual grains and the asperities that mark their contacts.

The first two terms on the right side of equation (1) describe the normal diffusion of heat towards cooler regions and the modifications to the temperature field that are produced by variations in the thermal conductivity. The source term is proportional to the product of the shear strength τ and the strain rate γ. The former is treated as proportional to the effective stress on the symmetry plane, assuming that the normal stress $\sigma_{yy} = -\sigma_N$ is constant so that

$$\tau = \mu\left[\sigma_N - P(0,t)\right], \tag{3}$$

where the choice of friction coefficient μ is discussed further below. We set $\gamma = V/h$, where the shear-zone thickness h and slip rate V will subsequently be treated as constants. The first two terms on the right side of equation (2) describe how the pore fluid diffuses outwards from the shear zone much as the heat does, but at a rate determined by the fluid transport and storage properties of the gouge, in addition to their lateral changes. The final term accounts for the capacity of temperature changes to drive changes in the pore pressure.

The thermal α_{th} and hydraulic α_{hy} diffusivities, and the expansion ratio Λ are all functions of the local pressure and temperature state. Specifically, $\alpha_{th} \equiv K/\rho c$, where the thermal conductivity K is treated as a function of temperature according to the empirical relation given by Vosteen and Schellschmidt [2003]; variations in the effective heat capacity $\rho c \approx 2.7$ MPa/°C are assumed negligible in comparison and treated using the value quoted by Lachenbruch [1980]. Changes in $\alpha_{th} \equiv k/(\eta\beta)$ are produced by i) the dependence of permeability k on pore pressure, represented with logarithmic fits to unloading data reported by Wibberley and Shimamoto [2003] and beginning at a nominal value of $k \approx 6.5 \times 10^{-21}\text{m}^2$ for the assumed ambient state at 7 km depth; ii) variations in fluid viscosity η with temperature and pressure, as interpolated from the values tabulated by Tödheide [1972]; iii) state-dependent changes to the storage capacity $\beta \equiv \phi(\beta_f + \beta_\phi)$, where the ratio ϕ of pore volume to gouge volume in the initial reference state, and the pore compressibility $\beta_\phi \equiv (1/\phi)\partial\phi/\partial P$ are both treated as pressure dependent and obtained from the laboratory data of Wibberley and Shimamoto [2003], while the fluid compressibility $\beta_f \equiv (1/\rho_f)\partial\rho_f/\partial P$ is calculated as a function of P and T from the ninth order polynomial fit to density data reported by Burnham et al. [1969]. The state dependence of $\Lambda \equiv (\lambda_f - \lambda_\phi)/(\beta_f + \beta_\phi)$ accounts as well for the pressure dependence of $\lambda_\phi \equiv (1/\phi)\partial\phi/\partial T$ based on the Wibberley and Shimamoto [2003] data, following the formulation of Rice [2006], while the polynomial fit to density data [Burnham et al., 1969] used for β_f is also employed to calculate the fluid expansivity $\lambda_f \equiv -(1/\rho_f)\partial\rho_f/\partial T$.

In the flash-weakening formulation of Rice [2006], the friction coefficient that results from slip on a surface with highly stressed asperity contacts is written as $\mu = \mu_0$ for $= V \le V_w$, and $\mu = (\mu_0 - \mu_w)\, V_w/V + \mu_w$ for $V > V_w$, where $\mu_0 = 0.6$ is the low-speed friction coefficient, and $\mu_w = 0.25$ is the high-speed, weakened friction coefficient. The critical slip rate for the onset of weakening is

$$V_w = \frac{\pi\alpha_{th}}{D_a}\left\{\frac{\rho c\left[T_w - T(0,t)\right]}{\tau_c}\right\}^2$$

where α_{th} is the thermal diffusivity evaluated at the temperature on the mid-plane, $D_a \approx 5 \times 10^{-6}$ m is a typical asperity size, $T_w \approx 900$ °C is the weakening temperature, and $\tau_c \approx 3$GPa is the contact shear strength. We compare two different approaches for extending this flash-weakening model to describe shear in a layer of finite width. In the first case, shown in figure 1(a), the relative motion between gouge particles in the shear zone is approximated as the product of the shear rate with the characteristic grain diameter D_g (below we take $D_g \approx D_a$). This leads to a friction model with $\mu = \mu_0$ for $\dot\gamma \le \dot\gamma_w$, and $\mu = (\mu_0 - \mu_w)\,\dot\gamma_w/\dot\gamma + \mu_w$ when $\dot\gamma > \dot\gamma_w$, where $\dot\gamma_w = V_w/D_g$. In the second case, as suggested by Rice [2006] and shown in figure 1(b), we view the finite shear zone as a manifestation of the geometrical requirements for accommodating extended slip within a polydisperse granular media. The slip at any given time is assumed to be localized to a surface. However, obstructions force this surface to move laterally during the course of a slip event, leading to an apparent finite shear width h. The frictional behavior implied by this scenario is approximated using the original flash-weakening formulation of Rice [2006], with μ written in terms of the velocity ratio V_w/V.

The parameter choices discussed above are appropriate when the gouge behaves elastically during the slip event. High stresses associated with the passage of the rupture front might be expected to cause significant modifications to the gouge properties [Poliakov et al., 2002; Andrews, 2005; Rice and Cocco, 2006]. In particular, this *damage* may serve to increase the permeability and alter the poroelastic behavior within the shear zone. We follow the procedure outlined by Rice [2006] to explore the magnitude of these effects in our state-dependent formulation by altering λ_ϕ, β_ϕ and k, as described further below.

3. MODEL RESULTS

We impose constant ambient initial temperature and pressure throughout the model domain, and zero flux conditions along the symmetry plane and at the far-field boundary. At the shear-zone boundary, where $y = h$, we impose continuity in T, P, heat flux, and mass flux. Equations (1) and (2)

are then solved in MATLAB using the method of lines [e.g. Schiesser, 1991] at uniformly spaced nodes that extend from the symmetry plane out to beyond the zones over which significant temperature and pressure changes occur. Space is discretized so that 5 nodes are within the shear layer.

3.1. The Effects of Flash Weakening on Thermal Pressurization

Figure 2 shows the normalized fault strength τ/τ_0 as a function of slip distance for three different cases, designed to illustrate the effects of flash-weakening. For an initial temperature of $T(0,0) = 210$ °C, the characteristic weakening velocity is $V_w \approx 0.17$ m/s. The dot-dashed line corresponds to the case where $\mu = \mu_w$, as is implied for slip-rates V that are much greater than V_w under the flash-weakening formulation of Rice [2006]. This is the anticipated behavior for the case of localized shear depicted in figure 1(b) at typical sesimic slip rates. Because the normalization is made with respect to the initial strength evaluated prior to weakening when $\mu = \mu_0$, at small slip distances $\tau/\tau_0 = \mu_w/\mu_0 \approx 0.42$. The solid line in figure 2 corresponds to the case where μ is a function of strain-rate $\dot{\gamma}$ and $\dot{\gamma}_w(T)$, as expected for the case of uniform shear depicted in figure 1(a). For a nominal slip-rate of $V = 1$m/s and shear width $h = 0.145$mm, the ambient temperature is sufficiently low that initially $\dot{\gamma} < \dot{\gamma}_w \approx 3 \times 10^4 s^{-1}$ and $\mu = \mu_0$. However, frictional heating causes the temperature to rise so that the value of $\dot{\gamma}_w$ decreases until it eventually falls below $\dot{\gamma} = V/h \approx 7 \times 10^3 s^{-1}$; μ then begins to fall towards μ_w, as shown with the dashed line. The dotted line displaying the calculation for constant $\mu = \mu_0$ is almost completely obscured by the solid curve for $\mu = \mu(\dot{\gamma})$. For the parameters chosen here, the predicted strength is relatively insensitive to the value of μ for slips that exceed several mm, and all three curves coincide thereafter. While a close correspondence at large slip and low strength is expected to be a general feature of the system behavior, the near-exact correlation seen here is somewhat fortuitous and must be partly attributed to the tendency of state-dependent property variations to reduce the gradient in pore pressure near the symmetry plane—thereby limiting the rate of strength evolution in comparison to what would be expected if these property variations were neglected.

Figure 3 shows the temperature along the symmetry plane as a function of slip distance for the three frictional models just described. The predicted temperature rise for $\mu = \mu_w$ is lower than that for the other two cases. However, the solid curve for $\mu = \mu(\dot{\gamma})$ begins to approach this limit at the larger slip distances that characterize the most significant seismic events. We note that the temperature remains lower than T_w for the calculations shown here. Because fluid flow reduces the rate at which the strength drops, however, the temperature rise is greater than that predicted by an idealized model in which the transport of heat and mass are neglected [Lachenbruch, 1980; see also Rempel and Rice, 2006]. At the smallest slip distances fluid and heat do not yet have time to escape the shear zone and the model predictions agree with those of the idealized model proposed by Lachenbruch [1980].

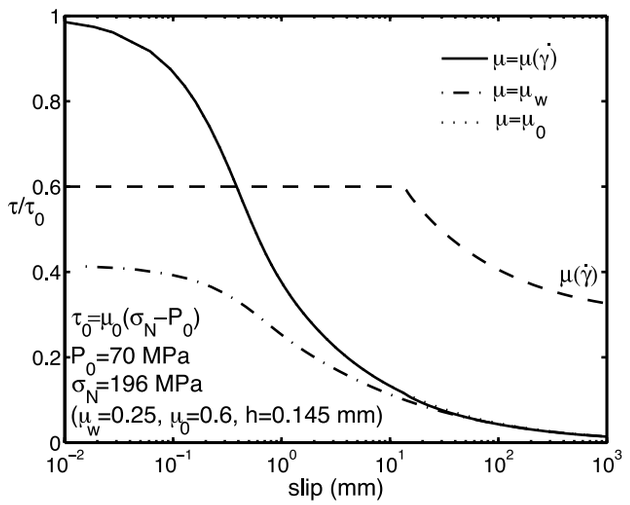

Figure 2. Fault strength normalized by $\tau_0 = \mu_0(\sigma_N - P_0)$. Results for three different models of frictional behavior are shown; note that the dotted line for $\mu = \mu_0$ is almost completely obscured by the solid line for $\mu = \mu(\dot{\gamma})$. The dashed curve shows the friction coefficient itself for the model in which the degree of flash weakening depends on strain rate and temperature.

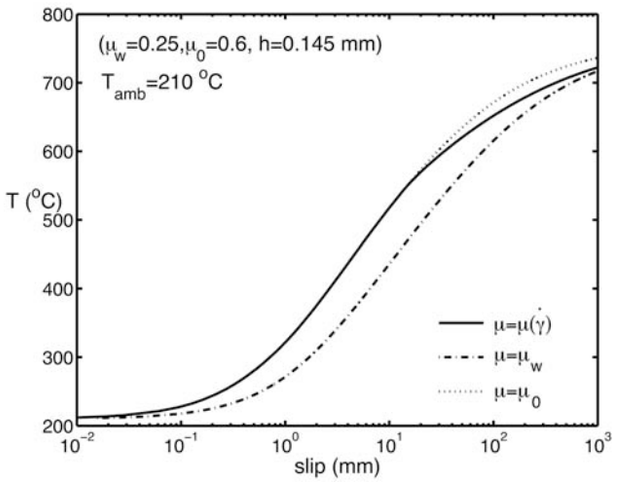

Figure 3. Temperature as a function of slip distance. A nominal ambient temperature of $T_{amb} = 210$ °C was chosen as representative of conditions at moderate seismogenic depths (e.g. 7km for a geothermal gradient of 30 °C/km).

The evolving pore pressure and temperature produce dramatic changes to the constituent properties. In figure 4 these effects are illustrated for the case where $\mu = \mu(\dot{\gamma})$ at a slip distance of 1m. The three labeled curves show the hydraulic diffusivity α_{hy}, thermal diffusivity α_{th}, and expansion ratio Λ as a function of distance y from the symmetry plane. For distances beyond the zone affected by heat and mass transport—the right side of the graph—these parameters remain at their ambient, initial values. The dashed line shows the influence of the rising temperature on the thermal conductivity, which leads to a reduction in α_{th} within the region of elevated temperatures, which extends out to y ≈ 3mm. The other two curves exhibit more complex behavior resulting from the dependence of several properties on both temperature and pore pressure—the latter effects extending out to distances approaching y ≈ 6mm. Most notable are the variations in fluid properties, particularly the viscosity, and density, which are influenced in opposite directions by the increases in P and T. Additionally, the hydraulic diffusivity is strongly influenced by the increased permeability at high pore pressures—this produces an order of magnitude increase in α_{hy} near the symmetry plane.

3.2. The Effects of Damage on Thermal Pressurization

The response of the pore volume to changes in P and T is controlled by the values of β_ϕ and λ_ϕ, which were obtained from isotropic, unloading experiments performed by [Wibberley and Shimamoto, 2003] on gouge from the Median Tectonic Line. Our model application requires that only σ_N remain constant, but that fault-parallel stress components evolve to keep fault-parallel strain components near zero. The results presented to this point have used values of β_ϕ and λ_ϕ that are inferred from the Wibberley and Shimamoto [2003] data under the assumption that the material adjacent to the shearing zone remains intact, elastic and isotropic. An alternative interpretation, motivated in part by the large predicted P and T changes, and in part by the recognition that the fault-wall material is likely to have been subject to inelastic deformation at the onset of rupture, motivates the calculations that follow. A detailed thermo-poroelastic analysis for both cases is given in the appendix of Rice [2006].

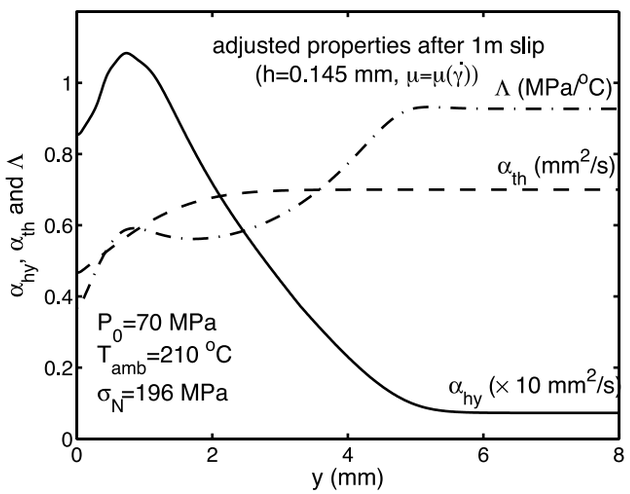

Figure 4. Property variations normal to the symmetry plane after a slip distance of 1m for the case where $\mu = \mu(\dot{\gamma})$, as shown by the solid curves in figures 2 and 3. Near the symmetry plane the hydraulic diffusivity is an order of magnitude larger than the thermal diffusivity so the scale on the y-axis should be multiplied by 10mm^2/s for α_{hy}. Ambient values for these parameters are those on the right side of the graph (e.g. $\Lambda \approx 0.93$ MPa/°C, $\alpha_{th} \approx 0.70$ mm^2/s, and $\alpha_{hy} \approx 0.73$ mm^2/s).

Fault-zone damage has the potential to drastically alter the state dependence of the pore volume fraction and lead to large increases in permeability. In particular, damage can ultimately lead to vanishingly small fault-parallel stress components, while the normal stress component remains fixed at $\sigma_{yy} = -\sigma_N$. Following Rice [2006], we account for these effects by taking $\lambda_\phi = \lambda_s$, where $\lambda_s \approx 2.4 \times 10^{-5}$ °C^{-1} is chosen to represent the thermal expansivity of the solid gouge particles; setting $\beta_\phi = \left(\beta_d^{dmg} - \beta_s\right)/\phi - \beta_s$, where $\beta_s \approx 1.6 \times 10^{-11}$ Pa^{-1} is a representative compressibility for the solid gouge particles and $\beta_d^{dmg} = m_a \beta_d$ is a multiple of the the drained compressibility β_d; and letting $k^{dmg} = m_k k$, where $m_k \geq 1$ is treated as a constant.

Figure 5 shows the evolution of fault-zone strength for a matrix of m_β and m_k values. The use of the strain-rate dependent flash-weakening formulation for these calculations is evidenced by the break in slope once the temperature becomes high enough that $\dot{\gamma} > \dot{\gamma}_w$ (approximately 500 °C here). The associated reduction in $\mu(\dot{\gamma})$ causes the fault strength to decrease more rapidly until $T = T_w = 900$ °C, beyond which $\mu = \mu_w$ was held constant. The ascending curves show the temperature rise to a limit of 1000 °C, which is considered representative of the onset of melting. Calculations beyond this point would require an expansion of the modeling effort to incorporate several fundamental physical effects that accompany the phase transition; these include the requirement that $P = \sigma_N$ as macroscopic melting occurs so that equation (3) no longer applies and further shear resistance must be attributed to the effective viscosity of the fluidized zone. The slip required for the onset of melting is reduced as the values of m_β and m_k increase and allow for additional fluid storage and/or expulsion from the shear zone. Over the range of m_β and m_k values studied,the energy released prior to melting ($E_m = \int_0^{D_m} \tau \mathrm{d}D$, where D_m is the slip at melt onset and τ_0=75.6 MPa here) decreases by a factor of 5, from $E_m \approx 2.7$MJ/m^2 at $D_m \approx 0.83$m for $k^{dmg} = k$, and $\beta_d^{dmg} = \beta_d$ to $E_m \approx 0.53$MJ/m^2 at $D_m \approx 0.024$m for $k^{dmg} = 10k$, and $\beta_d^{dmg} = 2\beta_d$.

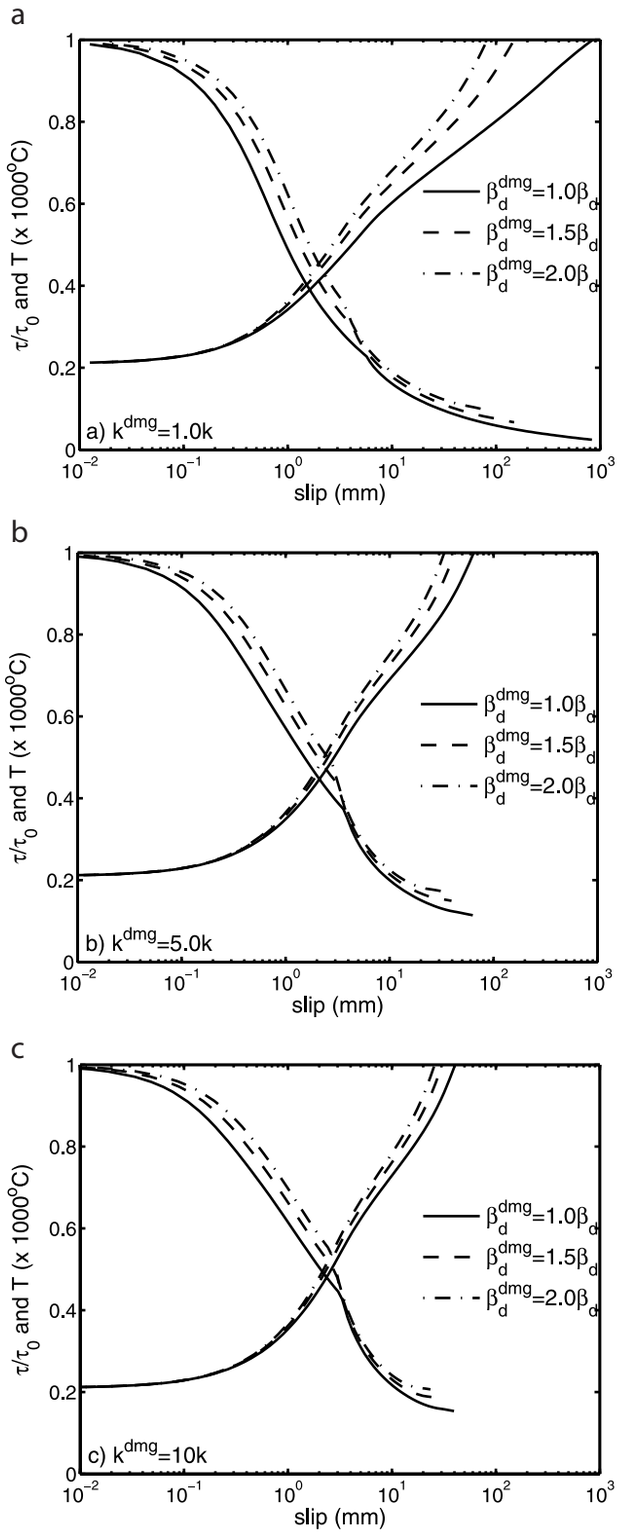

Figure 5. Normalized strength (decreasing) as a function of slip distance for parameters chosen to illustrate the effects of damage. The ascending curves show the temperature along the symmetry plane (plotted here to a maximum of 1000 °C, at which point the calculations were terminated). The three sets of curves in each plot differ in their choice of damaged pore compressibility β_d^{dmg}, treated here as a multiple of the drained compressibility β_d, as discussed in the text. The effect of damage on the permeability is represented as a multiple of the laboratory-derived k of Wibberley and Shimamoto [2003] so that in a) $k^{dmg} = 1.0k$, in b) $k^{dmg} = 5.0k$, and in c) $k^{dmg} = 10k$.

4. CONCLUSIONS

We have shown how the large changes in temperature and pore pressure that accompany earthquake slip dramatically alter fault-zone properties and influence the state evolution. The effects of flash weakening in a finite shear zone may also cause significant temporal variations in the friction coefficient. Simulations demonstrate that these changes have a comparatively minor influence on the fault strength at large slip, but they can be much more important in controlling the thermal evolution. Increases to the permeability and changes to the thermo-poroelastic behavior that are produced by damage promote increased fault strength and more rapid temperature rise. The slip required to achieve melting conditions is greatly reduced as the effects of damage become more pronounced. While the current model is not adequate to treat the subsequent evolution, the apparent scarcity of widespread melting along mature fault zones exhumed from moderate seismogenic depths [e.g. Sibson and Toy, 2006] can be interpreted as imposing limits on the degree of damage that typically takes place. Alternative explanations include the possibility that i) melts are generated but not preserved, ii) the ambient strength is lower than modeled here, iii) the typical width of the principal slip surface is greater than modeled here, iv) additional energy sinks significantly limit the temperature rise, or v) additional physical effects that accompany the phase transition conspire to limit subsequent melt production. With the exception of (v), each of these possibilities is discussed elsewhere in this volume.

Acknowledgments. Funds from the University of Oregon supported me during the writing of this manuscript, and a generous travel allowance from the U.S.G.S. helped offset the costs of attending the Chapman Conference in Portland. I thank Jim Rice for guiding my introduction to fault mechanics during my time at Harvard University and for constructive conversations since. Reviews by Paul Segal and Massimo Cocco, and the editorial comments of Art McGarr have greatly improved the final presentation.

REFERENCES

Andrews, D. J. (2002), A fault constitutive relation accounting for thermal pressurization of pore fluid, *J. Geophys. Res*., 107(B12), 2363, doi:10.1029/ 2002JB001942.

Andrews, D. J. (2005), Rupture dynamics with energy loss outside the slip zone, *J. Geophys. Res*., 110(B1), 1307, doi:10.1029/2004JB003191.

Beeler, N. M., and T. E. Tullis (2003), Constitutive relationships for fault strength due to flash-heating, USGS Open File Report, submitted.

Beeler, N. M., and T. E. Tullis (2006), Constitutive relationships and physical basis of fault strength due to flash-heating, this volume.

Bowden, F. P., and P. H. Thomas (1954), The surface temperature of sliding solids, *Proc. Roy. Soc. Lond., Ser. A*, 223 , 29–40.

Burnham, C. W., J. R. Holloway, and N. F. Davis (1969), *Thermodynamic Properties of Water to 1000°C and 10,000 bars*, Special Paper 132 (96 pp.), Geol. Soc. of Amer., Boulder Colo..

Bizzari, A., and M. Cocco (2006a), A thermal pressurization model for the spontaneous dynamic rupture propagation on a three-dimensional fault: 1. Methodological approach, *J. Geophys. Res*., 111, B05303, doi: 10.1029/2005JB003862.

Bizzari, A., and M. Cocco (2006b), A thermal pressurization model for the spontaneous dynamic rupture propagation on a 3-D fault: Part II—Traction evolution and dynamic parameters, *J. Geophys. Res*., 111, B05304, doi: 10.1029/2005JB003864.

Chester, F. M., and J. S. Chester (1998), Ultracataclasite structure and friction processes of the Punchbowl fault, San Andreas system, California, *Tectonophys*., 295, 199–221.

Chester, J. S., and D. L. Goldsby (2003), Microscale characterization of natural and experimental slip surfaces relevant to earthquake mcechanics, SCEC Annual Report for 2003.

Chester, J. S., A. K. Kronenberg, F. M. Chester, and R. N. Guillemette (2003), Characterization of natural slip surfaces relevant to earthquake mechanics, *EOS Trans. AGU*, 84(46), Fall Mtg. Suppl., Abstract S42C-0185.

Chester, F. M., Chester, J. S., Kirschner, D. L., Schulz, S. E., and J. P. Evans (2004), in *Rheology and Deformation in the Lithosphere at Continental Margins* (eds. Karner, G. D., B. Taylor, N. W. Driscoll, and D. L. Kohlstedt) Columbia University Press, New York.

Cocco, M., P. Spudich, and E. Tinti (2006), On the mechanical work adsorbed on faults during earthquake ruptures, this volume.

Di Toro, G., D. L. Goldsby and T. E. Tullis (2004), Friction falls towards zero in quartz rock as slip velocity approaches seismic rates, *Nature*, 427, 436–460.

Di Toro, G., T. Hirose, S. Nielsen, and T. Shimamoto (2006), Relating high-velocity rock-friction experiments to coseismic slip, this volume.

Goldsby, D. L. and T. E Tullis (2002), Low frictional strength of quaratz rocks at subseismic slip rates, *Geophys. Res. Lett*., 29(17), Art. No. 1844.

Hirose, T., and T. Shimamoto (2005), Growth of a molten zone as a mechanism of slip weakening of simulated faults in gabbro during frictional melting, *J. Geophys. Res*., (B5), Art. No. B05202, doi: 10.1029/ 2004JB003207.

Kanamori, H. and L. Rivera (2006), Energy partitioning during an earthquake, this volume

Lachenbruch, A. H. (1980), Frictional heating, fluid pressure and the resistance to fault motion, *J. Geophys. Res*., 85, 6097–6112.

Lockner, D., H. Naka, H. Tanaka, H. Ito, and R. Ikeda (2000), Permeability and strength of core samples from the Nojima fault of the 1995 Kobe earthquake, in *Proceedings of the International Workshop on the Nojima Fault Core and Borehole Data Analysis, Tsukuba, Japan, Nov 22-23, 1999*, (Eds. H. Ito, K. Fujimoto, H. Tanaka, and D. Lockner), USGS Open File Report 00-129, 147–152.

Mase, C. W., and L. Smith (1985), Pore-fluid pressures and frictional heating on a fault surface, *Pure Appl. Geophys*., 122, 583–607.

Mase, C. W., and L. Smith (1987), Effects of frictional heating on the thermal, hydrologic, and mechanical response of a fault, *J. Geophys. Res*., 92, 6249–6272.

Noda, H., and T. Shimamoto (2005), Thermal pressurization and slip-weakening distance of a fault: An example of the Hanaore fault, Southwest Japan, *Bull. Seismol. Soc. Am*., 95(4), 1224–1233.

Poliakov, A. N. B., R. Dmowska and J. R. Rice, Dynamic shear rupture interactions with fault bends and off-axis secondary faulting, *J. Geophys. Res., 107 (B11)*, cn: 2295, doi: 10.1029/2001JB000572, pp. ESE 6-1 to 6-18, 2002

Prakash, V. (2004), Pilot studies to determine the feasibility of using new experimental techniques to measure sliding resistance at seismic slip rates, SCEC Annual Progress Report for 2004.

Prakash, V., and F. Yuan (2004), Results of a pilot study to investigate the feasibility of using new experimental techniques to measure sliding resistance at seismic slip rates, *EOS Trans. AGU,* 85(47), Fall Meet. Suppl., Abstract T21D-02.

Rempel, A. W. and J. R. Rice (2006), Thermal pressurization and melting in fault zones, *J. Geophys. Res*., doi: 10/29/2006JB004314.

Rice, J. R. (1999), Flash heating at asperity contacts and rate-dependent friction, *EOS Trans. AGU*, 84(46), Fall Meet. Suppl., Abstract S41G-01.

Rice, J. R. (2006), Heating and weakening of faults during earthquake slip, *J. Geophys. Res*., doi:10.1029/2005JB004006.

Rice, J. R., and M. Cocco (2006), Seismic fault rheology and earthquake dynamics, in *The Dynamics of Fault Zones* (ed. M.R. Handy), Dahlem Workshop (Berlin, January 2005) Report 95, The MIT Press, Cambridge, MA, USA, publication expected 2006.

Rice, J. R., and J. W. Rudnicki (2006), Stability of spatially uniform, adiabatic, undrained shear of a fault zone, in preparation.

Roig Silva, C., D. L. Goldsby, G. Di Toro, and T. E. Tullis (2004), The role of silica content in dynamic fault weakening due to gel lubrication, *EOS Trans. AGU*, 85(47), Fall Meet. Suppl., Abstract T21D-06.

Schiesser, W. E. (1991), *The Numerical Method of Lines*, Academic Press, San Diego, 326p.

Segall, P., and J. R. Rice (1995), Dilatancy, compaction, and slip instability of a fluid-infiltrated fault, *J. Geophys. Res*., 100, 22155–22171.

Shipton, Z. K., A. M. Soden, J. D. Kirkpatrick, and A. M. Bright (2006a), How thick is a fault? Fault displacement–thickness scaling revisited, this volume.

Shipton, Z. K., J. P. Evans, R. E. Abercrombie, and E. E. Brodsky (2006b), The missing sinks: Slip localization in faults, damage zones, and seismic energy budgets, this volume.

Sibson, R. H. (1973), Interactions between temperature and pore-fluid pressure during earthquake faulting and a mechanism for partial or total stress relief, *Nature*, 243(126), 66–68.

Sibson, R. H. (2003), Thickness of the seismic slip zone, *Bull. Seism. Soc. Am*., 93, 1169–1178.

Sibson, R. H., and V. Toy (2006), The habitat of fault-generated pseudotachylyte: Presence vs. absence of friction melt, this volume.

Tödheide, K. (1972), Water at high temperatures and pressures, in: *Water: A Comprehensive Treatise VI The Physics and Physical Chemistry of Water*, (ed. F. Frank), Plenum Press, New York.

Tsutsumi, A. and T. Shimamoto (1997), High-velocity frictional properties of grabbro, *Geophys. Res. Lett*., 24, 699–702.

Tullis, T. E., and D. L. Goldsby (2003a), Flash melting of crustal rocks at almost seismic slip rates, *EOS Trans. AGU*, 84(46), Fall Meet. Suppl., Abstract S51B-05.

Tullis, T. E., and D. L. Goldsby (2003b), Laboratory experiments on fault shear resistance relevant to coseismic earthquake slip, SCEC Annual Progress Report for 2003.

Vosteen, H.-D., and R. Schellschmidt (2003), Influence of temperature on thermal conductivity, thermal capacity and thermal diffusivity for different types of rock, *Phys. Chem. Earth*, 28, 499–509.

Wibberley, C. A. J. (2002), Hydraulic diffusivity of fault gouge zones and implications for thermal pressurization during seismic slip, *Earth Planets Space*, 54 (11), 1153–1171.

Wibberley, C. A. J., and Shimamoto, T. (2003), Internal structure and permeability of major strike-slip fault zones: the Median Tectonic Line in Mie Prefecture, Southwest Japan, *J. Struct. Geol.*, 25, 59–78.

Wibberley, C. A. J., and T. Shimamoto (2005), Earthquake slip weakening and asperities explained by thermal pressurization, *Nature*, 436, 689–692.

A. W. Rempel, Department of Geological Sciences, University of Oregon, Eugene, OR 97403, USA. (rempel@uoregon.edu)